Nonlinear Dyn (2025) 113:15487–15502
https://doi.org/10.1007/s11071-025-10949-z

RESEARCH

Non-bifurcation regulation of chaos in a memristive Hopfield neural network

Xin Zhang · Chunbiao Li · Irene Moroz · Keyu Huang · Zuohua Liu

Received: 6 May 2024 / Accepted: 28 January 2025 / Published online: 14 February 2025

Abstract The construction of neural networks using memristors has been widely studied in the field of brain-like computing. However, there is a relative lack of research on the non-bifurcation regulation of chaos in memristive neural networks. In this paper, a 4D memristive Hopfield neural network (HNN) model with non-bifurcation regulation such as amplitude and offset control is constructed using an absolute value voltage-controlled memristor as a tractor, which can generate chaotic attractors with multiple control types. The multistability of the memristive HNN model is investigated by phase diagrams, Lyapunov exponent spectra, and basins of attraction. Numerical simulations show that the amplitude of partial neuron can be regulated by the memristor coupling parameters, and the internal parameters of the memristor can easily control the offset of neurons in the phase space. More interestingly, when symmetry breaking occurs, the neurons can be offset in different directions depending on the choice of initial values. This system provides the first dynamically controllable memristive HNN model. Finally, a hardware circuit is designed to obtain attractors of arbitrary amplitude or position by selecting the appropriate control resistors. The analog hardware implementation verifies the numerical simulation and the theoretical analysis.

Keywords Hopfield neural network · Memristor · Amplitude control · Offset boosting · Multistability

X. Zhang · K. Huang
School of Electronics and Information Engineering, Nanjing University of Information Science & Technology, Nanjing 210044, China

C. Li (✉)
School of Artificial Intelligence, Nanjing University of Information Science & Technology, Nanjing 210044, China
e-mail: chunbiaolee@nuist.edu.cn; goontry@126.com

I. Moroz
Mathematical Institute, University of Oxford, Oxford OX2 6GG, UK

Z. Liu
State Key Laboratory of Coal Mine Disaster Dynamics and Control, Chongqing University, Chongqing 400044, China

1 Introduction

In 1982, J.J. Hopfield introduced the Hopfield Neural Network (HNN) [1], an n-dimensional dynamical system composed of many neurons, distinct from other biological neural networks [2–4]. The hyperbolic tangent activation function enables the HNN to learn and store complex patterns, as explored in studies [5, 6]. The HNN has been widely applied in areas such as pattern recognition [7], control system [8], optimization [9], and associative memory [10]. Its nonlinear activation function generates rich brain-like dynamics, offering deeper insights into human neural

activity and advancing neuromorphic systems [11]. Recently, enhanced HNN models have emerged, exhibiting dynamical behaviors such as chaos [12], hyperchaos [13], and coexisting attractors [14, 15], broadening their applications in areas such as image encryption [16, 17], associative memory [18], brain-like bionic [19].

Recent interest in coexisting attractors within neural networks stems from their potential to reveal hidden learning capabilities. Coexisting attractors, which represent diverse oscillation states emerging from different initial conditions, are common in neural systems [20–22]. In artificial intelligence, the number of attractors correlates with a network's storage capacity; more coexisting attractors mean more memory patterns can be stored. Memristors, with their innate memory properties, have become crucial in emulating synapses in neural networks. Their integration enhances the alignment of patterns with coexisting attractors, such as chaos [23–25], hyperchaos [26, 27], and other dynamics [28]. Min et al. [29] derived three memristive HNNs with hyperbolic memristors, exhibiting anti-monotonicity and complex fractal structures due to coexisting attractors. Additionally, periodic function-type memristors facilitate the creation of line or surface equilibrium points, inducing homogeneous multistability [30]. Lin et al. [31] incorporated a sine memristor synapse into a four-dimensional HNN model, resulting in infinitely many coexisting attractors. Similarly, Lai et al. [32] introduced a multi-scroll memristive HNN by combining sinusoidal and hyperbolic tangent functions, enabling the generation of numerous coexisting attractors through periodic initial value selections. Lin & Wang [33] developed a 9D memristive HNN by interlinking two sub-HNN networks via a memristor, exhibiting hyperchaotic characteristics and extreme multistability based on initial values. This model has been effectively applied in biomedical image encryption. In summary, using memristor to model synapses stimulates complex dynamics, making it a hotspot in neuron research [34–36]. However, most current literature focuses on predictable homogeneous multistability based on periodic functions, while research on coexisting chaos and multi-periodic states remains relatively rare.

The non-bifurcation regulation of chaos, including amplitude control and offset boosting, has become a significant focus in nonlinear field heading to the controllability of chaos. Early chaos control is mainly based on the parameter modulation [37] and feedback [38], but all these do not regulate the internal properties of chaos like amplitude, offset, and frequency. Later, people began to study the non-bifurcation control leading to the development of chaos regulation [39–42]. The introduction of memristor has further expanded these possibilities [43], with new offset functions shifting control from system parameters to initial conditions [44]. This can trigger more multistability possibilities [45], such as attractor doubling [46], dynamic editing [47], and initial value-dominated uncountable many attractors [48]. In neural networks, amplitude control directly impacts input pattern recognition, enhancing the network's ability to distinguish and classify patterns. It enlarges the basin of attraction, improving adaptability to complex data, while offset boosting adjusts activation thresholds, increasing sensitivity to diverse inputs. This regulation is vital for maintaining efficient and accurate processing in uncertain conditions. Non-bifurcation regulation of firing, based on amplitude control and offset boosting, enhances memristive synapse capabilities, facilitating neuronal firing applications in electronic information and brain-like computing. However, the complex mathematical expressions in neuronal models pose challenges for non-bifurcation regulation, making the choice of an appropriate memristor model crucial for effective neural firing control.

Some memristor-based HNNs show multistability or give multi-scroll attractors, even some of which show easy amplitude control, but all those models resort to the parameters from other dimensions of the HNN model rather than the coupling coefficients or internal parameters of the memristor [49]. So in this manuscript, we introduce an innovative memristor-based HNN model, which is given the opportunity to modulate the firing of neural networks by the introduction of a memristor. The primary contributions of this study are as follows:

(1) A memristive HNN model is proposed and is enabled to generate complex coexistence behavior of attractors.
(2) The coupling weights of the memristor synapse can rescale the amplitude of the neural firing.
(3) The intermediate variables of the memristor can simultaneously regulate the amplitude and offset of

the neuron firing, and different modes of offset boosting can be realized depending on different initial values.

(4) An analog circuit was implemented to verify the theoretical analysis of the proposed memristive HNN, and the amplitude control and offset boosting were observed realistically on an oscilloscope.

In the following, the memristive HNN model is described in Section 2. Some basic analysis of dynamical behaviors is presented, including coexisting behaviors and bifurcation observation are proposed in Section 3. Section 4 reveals the amplitude control and offset boosting of the proposed HNN model. The hardware circuit is developed to verify the theoretical analysis in Section 5. Conclusion and discussion are given in the last section.

2 Design of memristive Hopfield neural network

A HNN can be used to simulate the spontaneous chaotic dynamics in the nervous system. The mathematical model of a HNN composing n neurons can be described as [1]:

$$C_i\dot{v}_i = -\frac{v_i}{R_i} + \sum_{j=1}^{n} w_{ij}\tanh(v_j) + I_i \ (i,j \in N^*). \tag{1}$$

where v_i represents the normalized membrane potential of the neuron, R_i is the membrane resistance of the neuron, $\tanh(v_j)$ represents the activation function of the neural network, I_i represents the external input current, the synaptic weight coefficient w_{ij} describing the connection strengths between neurons i and j (N^* represents any positive integer). It is worth noting that the synaptic weight w_{ij} directly affect the dynamics of HNN.

The neural synapses modeled by memristor can be used as the mutual feedback connectors for neurons, which effectively simulate the magnetic coupling relationship between different neurons. Among the currently used memristor models, the circuit structure of absolute-value memristor is relatively simple and easy to construct chaotic behaviors, therefore, in this system, we chose the classical absolute-value voltage-controlled memristor and modified the feedback term to make it closer to the expression of Hopfield neuron, which is described by,

$$\begin{cases} I = W(\varphi)V = (2|\varphi| - 1)V, \\ \dfrac{d\varphi}{dt} = -\varphi + c\tanh(\varphi) + V. \end{cases} \tag{2}$$

where I, $W(\varphi)$, V are the current, memductance function, and voltage of the proposed memristor, φ is the internal intermediate variable of the memristor, which also affects the state of the memristor.

Synapses play significance roles in signal exchange between neurons. The proposed memristor (2) can be used to simulate biological synapses between neurons. Therefore, based on Eq. (1), a HNN with three neurons can be obtained by replacing w_{31} by a memristor, as shown in Fig. 1. Selection of appropriate synaptic weight coefficients by trial-and-error method, the synaptic weight matrix can be expressed as:

$$W = \begin{bmatrix} w_{11} & w_{12} & w_{13} \\ w_{21} & w_{22} & w_{23} \\ w_{31} & w_{32} & w_{33} \end{bmatrix} = \begin{bmatrix} a & -1 & 0.45 \\ 3.2 & 1.5 & 0.97 \\ W(u) & 0 & 0 \end{bmatrix} \tag{3}$$

Substituting Eq. (2), (3) into Eq. (1), the topology between each node of the neural network can be shown in Fig. 1, where the output voltage of neuron 1 is defined as x, the output voltage of neuron 2 is defined as y, and the output voltage of neuron 3 is defined as z, the mathematical model of memristive HNN becomes:

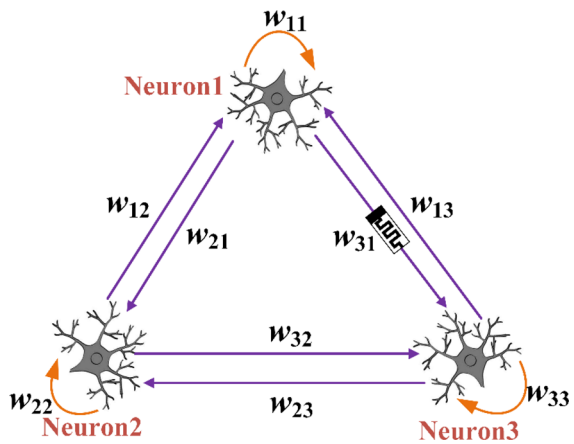

Fig. 1 The connection topology of the memristive HNN model

$$\begin{cases} \dot{x} = -x + a\tanh(x) - \tanh(y) + 0.45\tanh(z), \\ \dot{y} = -y + 3.2\tanh(x) + 1.5\tanh(y) + 0.97\tanh(z), \\ \dot{z} = -z - 12(2|u| - 1)\tanh(x), \\ \dot{u} = -u + c\tanh(u) + 1.5\tanh(x). \end{cases} \tag{4}$$

Here x, y, and z are the cell membrane potentials of the neurons, a is the control parameter, and c is the internal parameter of the memristor. When $a = 1.8$, and $c = 1.6$ under the initial condition (0.2, 0, 0, 0), the Eq. (4) are solved on ode45 algorithm with a step size of 0.005 and an iteration time of one thousand calculations in MATLAB, with the attractors are given in Fig. 2. The calculation of Lyapunov exponents (0.0653, 0, − 0.4329, − 0.9180) are based on the Wolf algorithm with a step size of 0.005 and million calculations in MATLAB. The calculation of the Kaplan-Yorke dimension can be derived from Eq. (5), where k is an integer and the LE_i are ordered so that the most positive or largest becomes LE_{i+1}. In this case, $LE_1 + LE_2 > 0$, but $LE_1 + LE_2 + LE_3 < 0$, so k is 2. Therefore, the Kaplan-Yorke dimension is $D_{KY} = 2.1508$.

$$D_{KY} = k + \frac{\sum_{i=1}^{k} LE_i}{LE_{k+1}} \tag{5}$$

Equation (4) is invariant under the transformation $(x, y, z, u) \leftrightarrow (-x, -y, -z, -u)$, showing rotational symmetry, which provides a possibility for coexisting symmetrical chaotic attractor trajectories in the phase space.

The equilibrium points of Eq. (4) can be calculated by setting the right side of Eq. (4) to zero:

$$\begin{cases} -x + a\tanh(x) - \tanh(y) + 0.45\tanh(z) = 0, \\ -y + 3.2\tanh(x) + 1.5\tanh(y) + 0.97\tanh(z) = 0, \\ -z - 12(2|u| - 1)\tanh(x) = 0, \\ -u + c\tanh(u) + 1.5\tanh(x) = 0. \end{cases} \tag{6}$$

Obviously, we cannot get an accurate analytical solution for the transcendental equation. But, Eq. (6) can be solved based on graphic analysis. First, Eq. (6) is changed to,

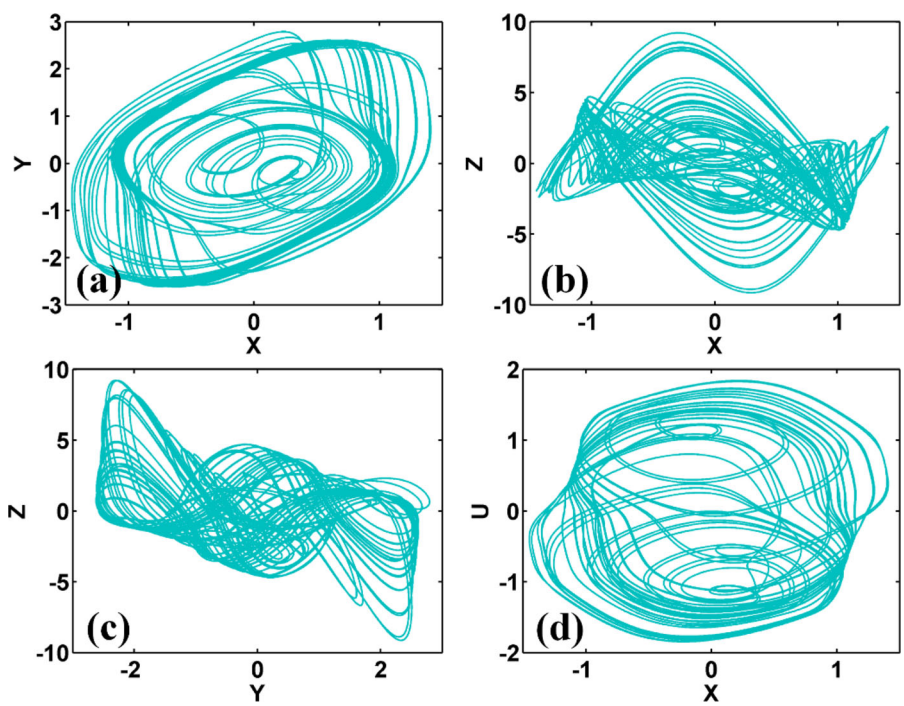

Fig. 2 Chaotic attractors of Eq. (4) when $a = 1.8$, and $c = 1.6$ under initial condition [0.2, 0, 0, 0]: **a** x–y plane, **b** x–z plane, **c** y–z plane, **d** x-u plane

$$\begin{cases} x = \operatorname{artanh}\left(\frac{2}{3}(u - c\tanh(u))\right), \\ z = -8(2|u| - 1)(u - c\tanh(u)), \\ f_1(y,u) = -x + a\tanh(x) - \tanh(y) + 0.45\tanh(z) = 0, \\ f_2(y,u) = -y + 3.2\tanh(x) + 1.5\tanh(y) + 0.97\tanh(z) = 0. \end{cases} \tag{7}$$

When $a = 1.8$, and $c = 1.6$, the solutions of Eq. (6) are ultimately related to the variables y and u. Therefore, by plotting the solutions of $f_1(y, u) = 0$ and $f_2(y, u) = 0$ in the graph, their intersections are the equilibrium points. The corresponding equilibrium points are shown in Fig. 3.

Although we see nine intersections in Fig. 3, but the intersections on the left and right are not equilibrium point solutions in the real number region due to the boundedness of the hyperbolic function. Therefore there are only 7 equilibrium points in Eq. (4). Their corresponding eigenvalues and their stabilities are shown in Table 1. The results of the numerical calculations indicate that all of the equilibrium points are unstable saddle-foci, which implies that the attractors in the memristive HNN are self-excited ones.

3 Initial-controlled coexisting behaviors

Because of the intrinsic memory and non-volatility effect of the memristor, many memory systems show sensitivity to initial conditions [49, 50]. Synapses simulated by a memristor can invoke different memory patterns in neuronal networks. In this subsection, coexisting attractors are revealed by means of research methods such as Lyapunov exponents, basin of attractions, and phase orbits.

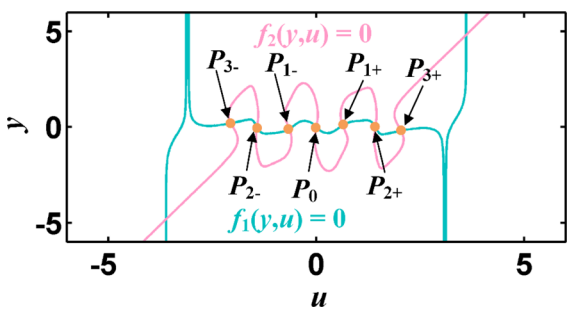

Fig. 3 Distribution of equilibrium points of Eq. (4) when $a = 1.8$, and $c = 1.6$

Fixing the memristive HNN parameters as $a = 1.8$, $c = 1.6$, $x_0 = 0.2$, $y_0 = 0$, $z_0 = 0$, when u_0 varies in $[-5, 5]$, the first three Lyapunov exponent spectra and bifurcation diagrams are shown in Fig. 4. The variance Lyapunov exponents show that the given system can exhibit rich dynamical behaviors under different initial values, including chaos, period-1, and period-3 behaviors.

To better illustrate the coexisting behavior of attractors, the phase trajectories under different initial values are shown in Fig. 5a, b. In order to reveal the influence of the initial values on the dynamics of the system, the basins of attractions are shown in Fig. 5c, d, where different color blocks have complex fractal structures: dark turquoise color represents the chaotic phase orbit, brown and orange color represent the symmetric attractor of period-3, blue and red color represent the symmetric attractor of period-1. Since the system is symmetric with respect to x-y-z-u, so the fractal structure of the basin of attractions also shows symmetry properties.

When the synaptic weight is changed, the coexisting behavior of the memristive HNN will also change. For $c = 2$, the complete attractor splits into two symmetric chaotic attractors, accompanied by symmetric period-2 coexisting attractors, the corresponding phase orbits are shown in Fig. 6a. The basin of attraction on the initial space of x_0-u_0 plane is shown in Fig. 6b, which also shows the rotational symmetry property with respect to the x-u dimension.

In addition to the coexistence of chaos and periodic states, there also exist different periodic states under specific parameters. With the synaptic weights fixed as $a = 2$, and $c = 1.7$, the chaotic behavior of the neural network begins to degenerate into periodicity, and the operation state of the network becomes the coexistence of symmetric pair of period-1 and period-4. The corresponding phase trajectories and the basin of attraction in the x_0-u_0 plane are shown in Fig. 7.

Three coexisting attractors are also found, as shown in Fig. 8, and it is worth noting that the system always produces pairs of attractors regardless of the change in synaptic weights. Overall, these results show that the dynamical behavior in memristor neural networks strongly depends on the initial state of synapses. This is an important way to understand how the nervous system works.

Table 1 Equilibrium points of Eq. (4) and their stability

Equilibrium points	Eigenvalues	Stabilities
P_0 $(0,0,0,0)$	$\lambda_1 = 0.6$	Index-3 Unstable Saddle focus
	$\lambda_2 = -2.9008$	
	$\lambda_{3,4} = 1.6004 \pm 1.9035i$	
P_{1+} $(-0.1777, 0.0993, 0.5901, 0.6398)$	$\lambda_{1,2} = -0.5003 \pm 1.5562i$	Index-2 Unstable Saddle focus
P_{1-} $(-0.1777, -0.0993, -0.5901, -0.6398)$	$\lambda_{3,4} = 0.6600 \pm 1.2200i$	
P_{2+} $(0,0,0,1.425)$	$\lambda_1 = -0.6692$	Index-1 Unstable Saddle focus
P_{2-} $(0,0,0,-1.425)$	$\lambda_2 = 1.5967$	
	$\lambda_{3,4} = -0.6483 \pm 3.7336i$	
P_{3+} $(0.3462, -0.1990, -12.3631, 2.0470)$	$\lambda_1 = -1$	Index-2 Unstable Saddle focus
P_{3-} $(-0.3462, 0.1990, 12.3631, -2.0470)$	$\lambda_2 = -0.8968$	
	$\lambda_{3,4} = 0.5213 \pm 1.6520i$	

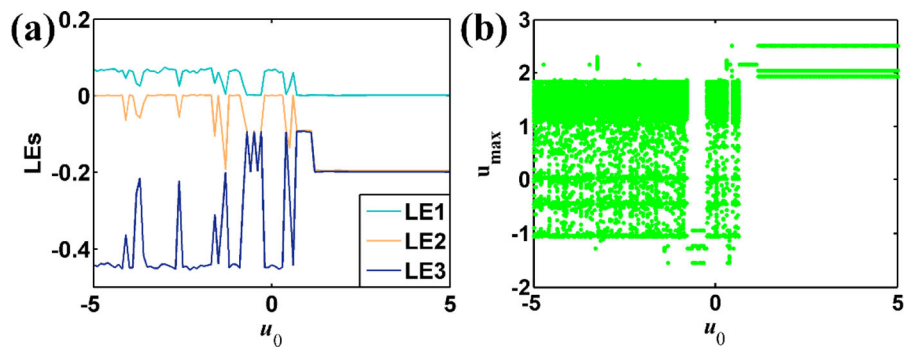

Fig. 4 Dynamic evolution of Eq. (4) with $a = 1.8$, and $c = 1.6$ under the initial condition $[0.2, 0, 0, u_0]$: **a** Lyapunov exponents, **b** Bifurcation diagrams

4 Non-bifurcation regulation of neural firing

The additional non-bifurcation regulatory functionality brought by memristor in dynamical systems plays an important role. However, it has not been observed in memristive neural networks. Surprisingly, the proposed memristor HNN can provide some special tuning to revise the properties of the signals. In this section, the basic analysis method is used to reveal the complex dynamic regulation of memristive HNN, including amplitude control and offset boosting.

4.1 Amplitude control

In the HNN, the nonlinear term is provided by the hyperbolic tangent function. When considering the amplitude control of the signal, we need to satisfy the term balance in the system, and then take the transformation $(x, y, z, u) \rightarrow (x, y, \frac{z}{m}, u)$, obtain to,

$$\begin{cases} \dot{x} = -x + a\tanh(x) - \tanh(y) + 0.45\tanh\left(\frac{z}{m}\right), \\ \dot{y} = -y + 3.2\tanh(x) + 1.5\tanh(y) + 0.97\tanh\left(\frac{z}{m}\right), \\ \dot{z} = -z - 12m(2|u| - 1)\tanh(x), \\ \dot{u} = -u + c\tanh(u) + 1.5\tanh(x). \end{cases} \tag{8}$$

Since the hyperbolic tangent function can be approximately equivalent to the sign function, we replace the $\tanh(\frac{z}{m})$ term in the first two dimensions with $\tanh(z)$, and reassign the memristor synapse weight as m. Then the system becomes:

$$\begin{cases} \dot{x} = -x + a\tanh(x) - \tanh(y) + 0.45\tanh(z), \\ \dot{y} = -y + 3.2\tanh(x) + 1.5\tanh(y) + 0.97\tanh(z), \\ \dot{z} = -z - m(2|u| - 1)\tanh(x), \\ \dot{u} = -u + c\tanh(u) + 1.5\tanh(x). \end{cases} \tag{9}$$

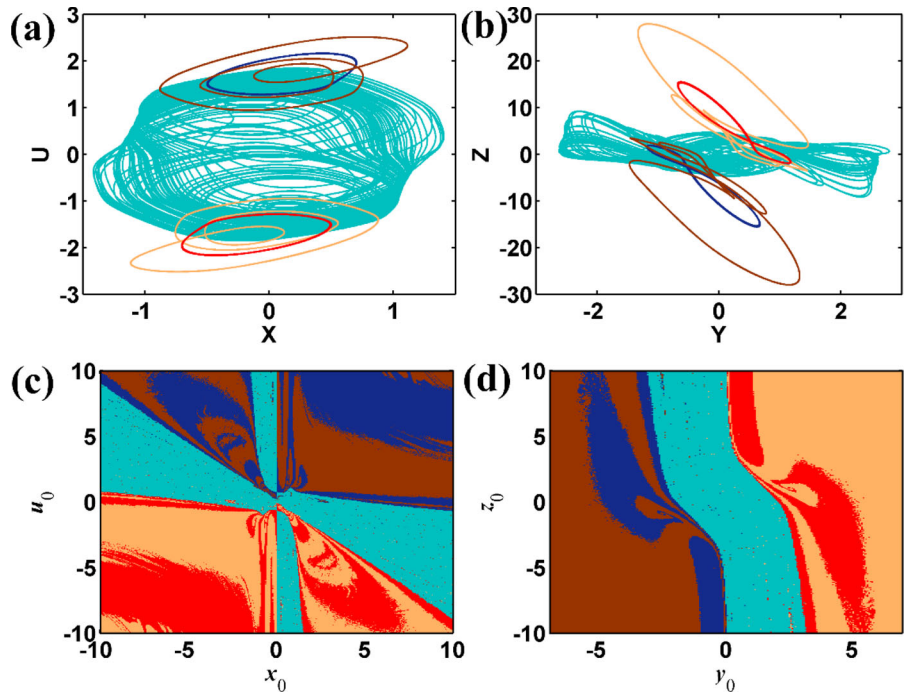

Fig. 5 Multistability behaviors of Eq. (4) with $a = 1.8$, and $c = 1.6$: **a** coexisting attractors in the x-u plane, **b** coexisting attractors in the y–z plane, **c** basin of attraction in the x_0–u_0 plane, cross section $y_0 = z_0 = 0$, **d** basin of attraction in the y_0–z_0 plane, cross section $x_0 = u_0 = 0$. IC1 = [0.2, 0, 0, 0] (dark turquoise), IC2 = [0.2, 0, 0, 1] (dark blue), IC3 = [0.2, 0, 0, 2] (brown), IC4 = [− 0.2, 0, 0, − 1] (red), IC5 = [− 0.2, 0, 0, − 2] (orange)

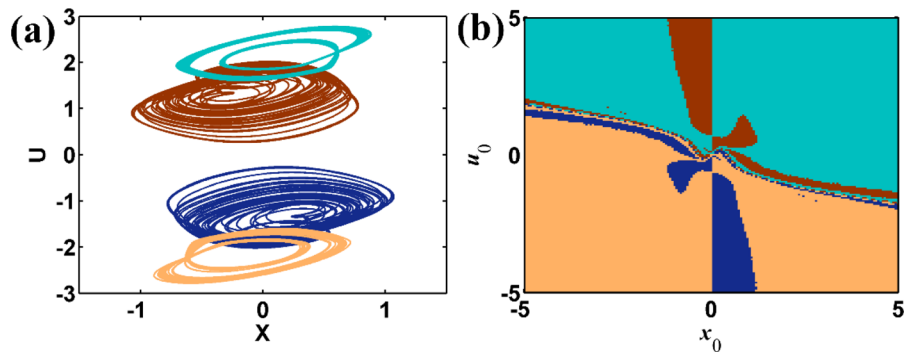

Fig. 6 Multistability behaviors of Eq. (4) with $a = 1.8$, and $c = 2$: **a** coexisting attractors on the x-u plane, **b** basin of attraction in the x_0–u_0 plane, cross section $y_0 = z_0 = 0$. IC1 = [0.1, 0, 0, 1] (dark turquoise), IC2 = [− 0.1, 0, 0, 0] (brown), IC3 = [0.1, 0, 0, 0] (blue), IC4 = [− 0.1, 0, 0, − 1] (orange)

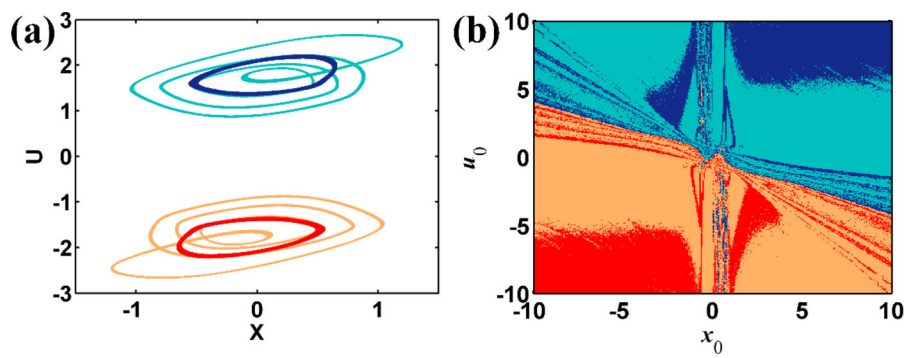

Fig. 7 Multistability behaviors of Eq. (4) with $a = 2$, and $c = 1.7$: **a** coexisting attractors on the x-u plane, **b** basin of attraction in the x_0-u_0 plane, cross section $y_0 = z_0 = 0$. IC1 = [− 0.1, 0, 0, 0] (dark turquoise), IC2 = [− 0.1, −1, 0, 0] (blue), IC3 = [0.1, 0, 0, 0] (orange), IC4 = [0.1, 1, 0, 0] (red)

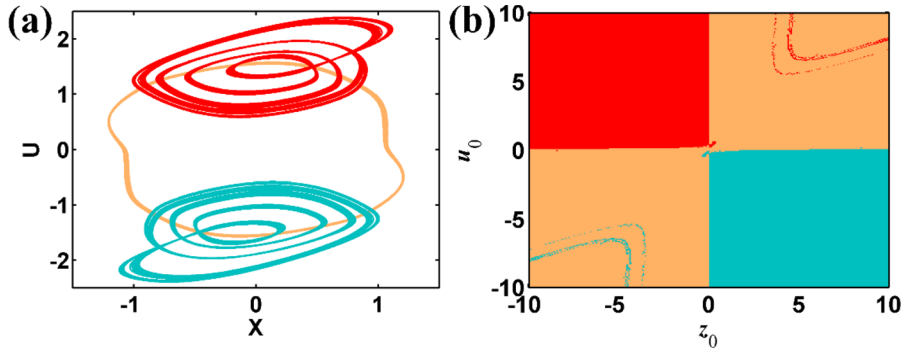

Fig. 8 Multistability behaviors of Eq. (4) with $a = 2$, and $c = 1.5$: **a** coexisting attractors on the x-u plane, **b** basin of attraction in the z_0-u_0 plane, cross section $x_0 = y_0 = 0$. IC1 = [− 0.1, 0, 0, 0] (dark turquoise), IC2 = [− 0.1, 1, 0, 0] (blue), IC3 = [0.1, 0, 0, 0] (orange)

Therefore, the memristor synaptic weight will indirectly change the amplitude of the neural z. However, the parameter m is not a non-bifurcation parameter due to the approximation used. When the memristor synapse weight m changes, the amplitude of the neural signal z will also change linearly, accompanied by a transition of the system dynamics.

To further explore the moderation effect of the synaptic weight m on the neural signal z, the Lyapunov exponent spectrum as m varies in the range [10, 50] is presented in Fig. 9a. Given that the memristive HNN exhibits coexisting chaotic and periodic attractors when $a = 1.8$, and $c = 2$, the amplitude and position of these attractors in phase space are different. Even though the initial values have been adjusted according to the basin of attraction, the system switches between periodic and chaotic oscillations when the amplitude parameter varies under a specified initial condition. The mean value of the neural signal z as a function of synaptic weight m is depicted in Fig. 9b. The figure reveals that the linear increase in the mean value can be divided into two distinct zones: a growth process with a small slope, which corresponds to the amplitude control of the symmetric pair of coexisting chaotic attractors, and a growth process with a large slope, which corresponds to the amplitude control of the symmetric pair of coexisting periodic attractors. The phase trajectories under different synapse weight m are shown in Fig. 10.

4.2 Offset boosting

After a more intensive study, it was found that, the amplitude of neural firing controlled by the memristor synaptic weights varies with the internal parameter c of the memristor. The phase trajectories in the x–z plane under different parameters c are shown in Fig. 11, and a phenomenon similar to Fig. 10 is observed, where the system also performs amplitude control in the case of broken symmetry when the parameters are varied.

After the simulation, it is found that the memristor HNN can hardly maintain a complete symmetric chaotic state as shown in Fig. 2, and the complete attractor breaks into two unipolar attractors in the u direction when the control parameter is slightly

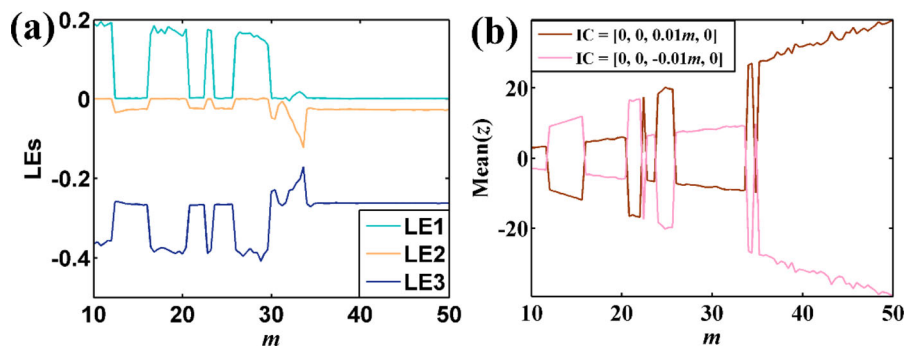

Fig. 9 Dynamic behaviors of Eq. (9) with $a = 1.8$, and $c = 2$: **a** Lyapunov exponents, **b** Average value of the signal z(t)

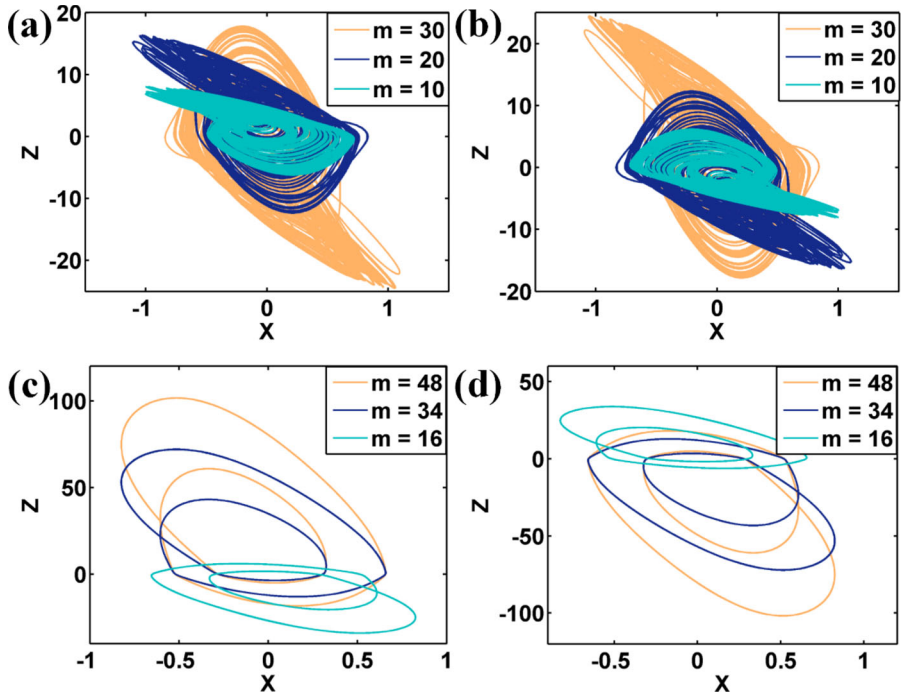

Fig. 10 Rescaled phase trajectories of Eq. (9) with $a = 1.8$, and $c = 2$ under different parameters of m: **a**, **c** IC1 = [0, 0, 0.01 m, 0], **b**, **d** IC2 = [0, 0, − 0.01 m, 0]

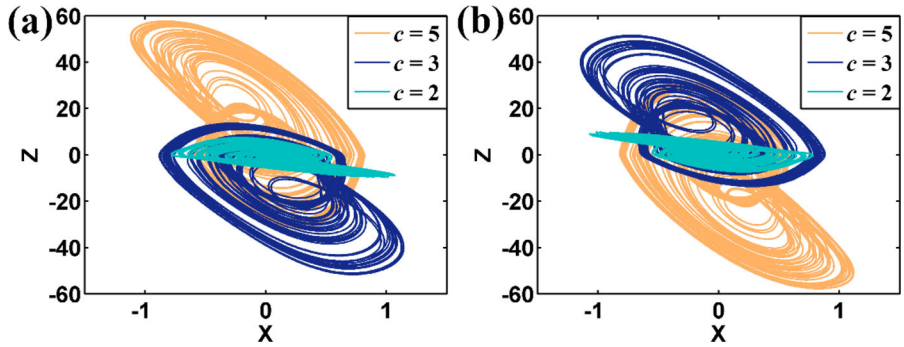

Fig. 11 Rescaled phase trajectories of Eq. (4) with $a = 1.8$ under different parameter c: **a** IC1 = [0.1, 0, 0, 0], **b** IC2 = [− 0.1, 0, 0, 0]

perturbed. In the case of broken symmetry, the variable u is unipolar, where $\tanh(u)$ is approximately equal to 1 or − 1. Therefore, in this case, we can take the parameter c as the offset constant of the internal variable u of the memristor, as discussed in detail in the following.

When the variable u is in the positive range, then $|u| = u$, taking $u \to u' - d(d > 0)$, the memristor can be simplified to,

$$\begin{cases} I = (2u' - 2d - 1)\tanh(x), \\ \dot{u'} = -u' + (c + d) + 1.5\tanh(x). \end{cases} \tag{10}$$

When the variable u is in the negative range, then $|u| = -u$, such that $u \to u' + d(d > 0)$, the memristor can be simplified to,

$$\begin{cases} I = (-2u' - 2d - 1)\tanh(x), \\ \dot{u'} = -u' - (c + d) + 1.5\tanh(x). \end{cases} \tag{11}$$

Combining the above two cases, when broken symmetry occurs, and the corresponding attractors are shifted by d units in their respective directions, then the memristor can be described as:

$$\begin{cases} I = (2|u| - 2d - 1)\tanh(x), \\ \dot{u} = -u + (c + d)\tanh(u) + 1.5\tanh(x). \end{cases} \tag{12}$$

In fact, varying the parameter c essentially shifts the unstable equilibrium of the memristor [25, 26]. Offset boosting can be obtained from the dimension of u based on the parameter c. In terms of the phase trajectory, the parameter c primarily affects the position of the attractor when symmetry is broken.

As demonstrated in the previous section, changes in the memristive synapse can adjust the amplitude of neuron z, while variations in the memconductance also indirectly affect the memristor synapse. Consequently, the internal parameter c of the memristor can influence both the amplitude of neuron z and cause an offset boosting in the variable u. The Lyapunov exponent spectrum of the parameter c varying in [1, 10] is shown in Fig. 12a, when the parameter c is too small, the broken symmetry of the attractor does not trigger the generation of a unipolar signal, indicating that the parameter c essentially acts as a bifurcation parameter within this limited range. However, as the parameter c gradually increases, the broken symmetry leads to the generation of a unipolar signal, transforming parameter c into a parameter where both amplitude control and offset control coexist. The corresponding mean value of all neurons under different values of parameter c are shown in Fig. 12b, where it can be observed that the average values of neuron z and the variable u increase in with different slopes.

Figure 13 illustrates how the parameter c affects the offset of the variable u. Due to the existence of symmetric multistability, there are four coexisting attractors for a fixed parameter c. For the robustness of the control, the corresponding initial values need to be changed according to the parameter c. This adjustment allows each class of attractors to boost in their respective directions based on different initial values.

5 Hardware experiments

The use of hardware circuits to implement the memristive HNN model can facilitate the design of neural networks more effectively. In this section, a circuit experiment implementing the memristive HNN model is used to verify the above theoretical results. For the proposed memristor HNN model, the nonlinearity provided by the hyperbolic tangent function is the main driver of chaos generation and is also the core module of the circuit implementation. This function is realized using 2 operational amplifiers, 4 transistors, and 11 resistors. Based on the hyperbolic tangent function module, a PCB board was constructed to implement the memristive HNN, which contains resistors, capacitors, operational amplifiers (type LM741CN), triode (type MPS2222), a four-quadrant analog multiplier (type AD633JN), and the circuit is supplied with ± 15 V. The analog circuit design for Eq. (4) is shown in Fig. 14, for the corresponding circuit equations:

$$\begin{cases} C_1\dfrac{du_{C_1}}{dt} = -\dfrac{1}{R_4}u_{C_1} + \dfrac{1}{R_1}\tanh(u_{C_1}) - \dfrac{1}{R_2}\tanh(u_{C_2}) + \dfrac{1}{R_3}\tanh(u_{C_3}), \\ C_2\dfrac{du_{C_2}}{dt} = -\dfrac{1}{R_8}u_{C_2} + \dfrac{1}{R_6}\tanh(u_{C_1}) + \dfrac{1}{R_5}\tanh(u_{C_2}) + \dfrac{1}{R_7}\tanh(u_{C_3}), \\ C_3\dfrac{du_{C_3}}{dt} = -\dfrac{1}{R_{10}}u_{C_3} - \dfrac{1}{R_9}i. \end{cases} \tag{13}$$

The equivalent circuit equations of the proposed memristor are:

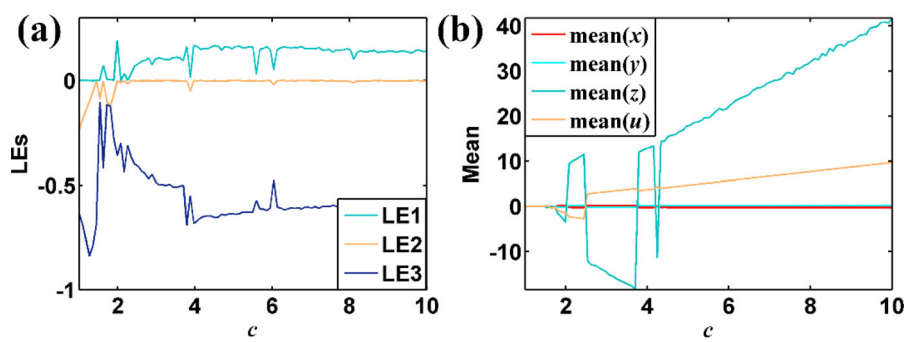

Fig. 12 Dynamic behaviors of Eq. (4) with $a = 1.8$ under initial condition IC = [0.1, 0, 0, 0]: **a** Inneural Lyapunov exponents, **b** Average value of the signals

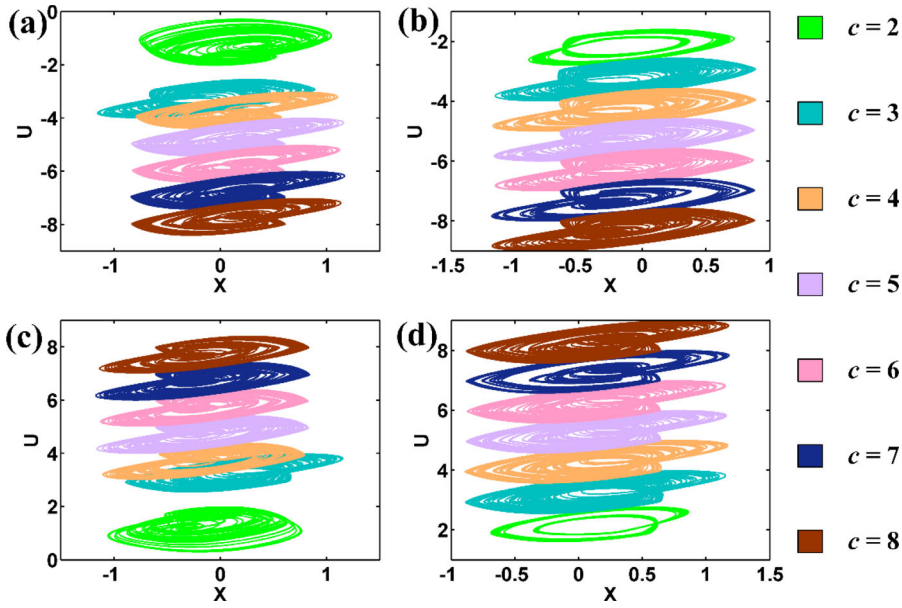

Fig. 13 Offset boosting of Eq. (4) with $a = 1.8$ under the parameter c:
a IC1 = [0.1, 0, 0, − c],
b IC2 = [− 0.5, 0, 0, − c],
c IC3 = [− 0.1, 0, 0, c],
d IC4 = [0.5, 0, 0, c]

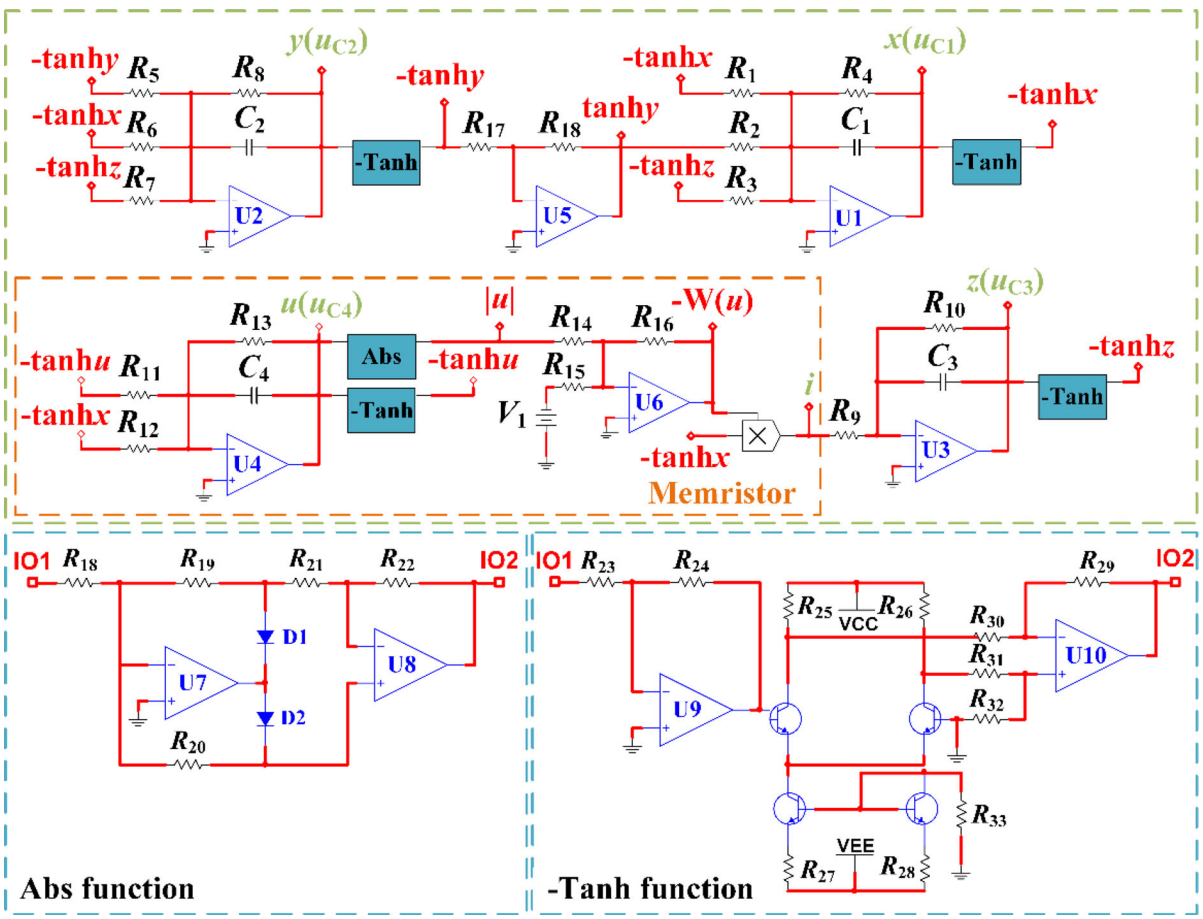

Fig. 14 The circuit schematic of the memristive HNN

$$\begin{cases} i = W(u)\tanh(x) = \left(\dfrac{R_{23}}{R_{21}}|u_{C_4}| - \dfrac{R_{23}}{R_{22}}V_1\right)\tanh(u_{C_1}), \\ C_4\dfrac{du_{C_4}}{dt} = -\dfrac{1}{R_{13}}u_{C_4} + \dfrac{1}{R_{11}}\tanh(u_{C_4}) + \dfrac{1}{R_{12}}\tanh(u_{C_1}). \end{cases} \tag{14}$$

In Eq. (14), is realized by a separate module. The inner variable u represents the internal state of the memristor, but in the simulation, it also corresponds to the capacitor voltage. According to the synaptic weight matrix of the memristive HNN given in Eq. (3), the corresponding circuit element parameters of Eq. (13) can be selected as $C_1 = C_2 = C_3 = 10$ nF, $R_1 = 5.5$ kΩ, $R_3 = 22\ k\Omega$, $R_2 = R_4 = R_7 = R_8 = R_{10} = R_{17} = R_{18} = 10$ kΩ, $R_5 = 6.5\ k\Omega$, $R_6 = 3.5\ \Omega$, $R_9 = 833\Omega$. The corresponding equivalent circuit parameters of the memristor in the orange dashed box are: $C_4 = 10$ nF, $R_{11} = 2$ kΩ, $R_{12} = 5$ kΩ, $R_{13} = R_{15} = R_{16} = 10$ kΩ, $R_{14} = 5$ kΩ, $V_1 = 1$ V. The corresponding equivalent circuit parameters of the absolute value function in the blue dashed box are:$R_{18} = R_{19} = R_{20} = R_{21} = R_{22} = 10$ kΩ, and the corresponding circuit element parameters of the -Tanh function can be fixed as: $R_{23} = R_{29} = R_{30} = R_{31} = R_{32} = 10$ kΩ, $R_{24} = 520\ \Omega$, $R_{25} = R_{26} = 1$ kΩ, $R_{27} = R_{28} = 2$ kΩ,$R_{33} = 9.8$ kΩ.

When the circuit elements are set to the above parameters, we observe a typical chaotic attractor similar to the numerical simulation on the digital oscilloscope (SIGLENT SDS 1102X), as shown in Fig. 15. By comparing Eq. (13) with Eq. (4), we know that resistor R_9 corresponds to the amplitude control parameter m in the mathematical model. By adjusting the resistor R_9, we can observe attractors at different scales on the oscilloscope. Figure 16 shows the amplitude control behaviors of z(t). Since the initial values are not easily controllable in the hardware circuit, the multistability behavior can only be observed by multiple switches as well as by touching the capacitor.

From the circuit, it can be seen that the resistor R_{11} corresponds to the offset control parameter c, it also brings the opportunity for amplitude control. The rescaled phase orbits under different R_{11} values with different initial conditions are shown in Fig. 17. The actual offset boosting behaviors of u(t) under different R_{11} are shown in Fig. 18. The PCB experimental results are photographed from the oscilloscope shown

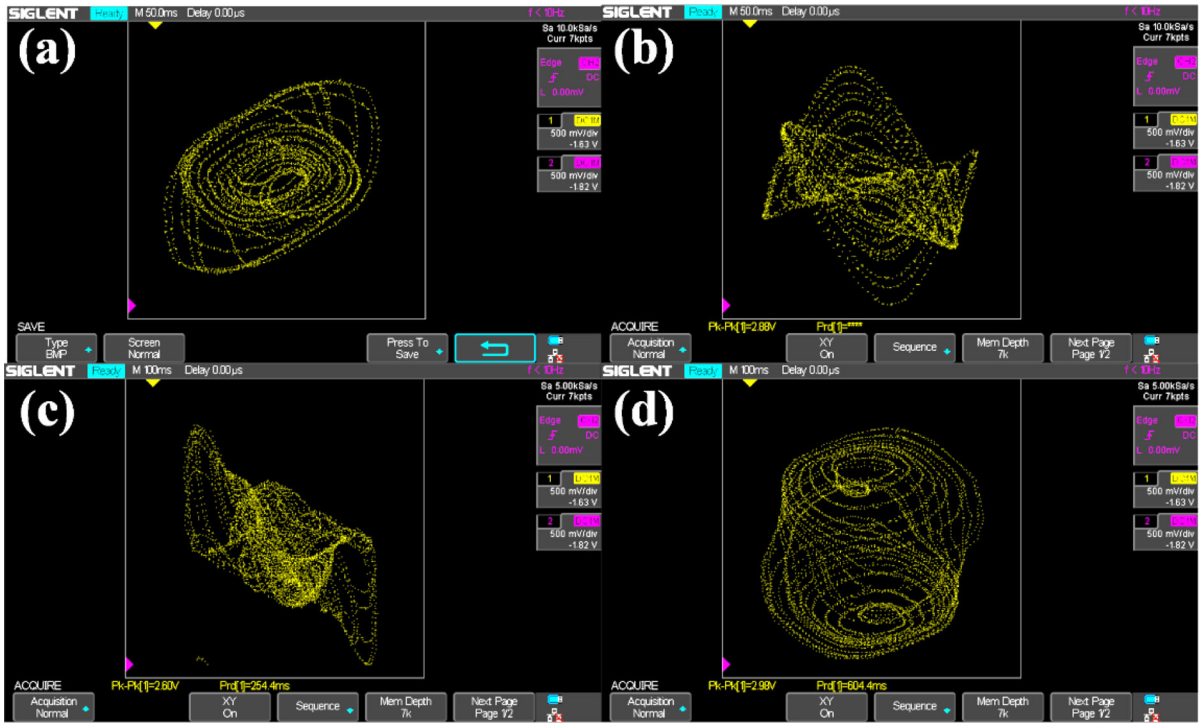

Fig. 15 The experimental circuit the memristive chaotic HNN. **a** x–y plane. **b** x–z plane. **c** y–z plane. **d** x-u plane

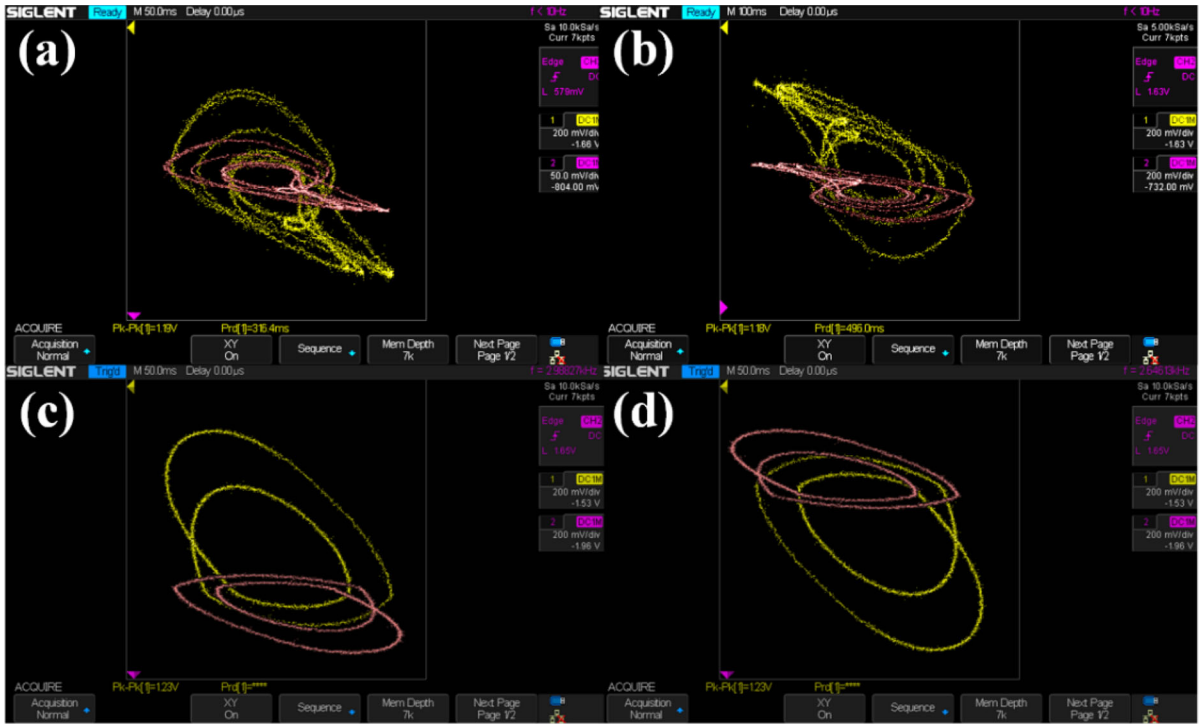

Fig. 16 Amplitude control observed on the oscilloscope by adjusting R_9 under different initial conditions. **a**, **b** $R_9 = 833\ \Omega$ (yellow), $R_9 = 500\ \Omega$ (red). **c**, **d** $R_9 = 200\ \Omega$ (yellow), $R_9 = 615\ \Omega$ (red)

Fig. 17 Amplitude control observed on the oscilloscope by adjusting R_{11} under different initial conditions. $R_{11} = 3.2\ \text{k}\Omega$ (yellow), $R_{11} = 5\ \text{k}\Omega$ (pink)

in Fig. 19. It should be noted that the resistance values in the actual circuit are not exactly equal to the ideal values because of the accuracy error between devices, but all other parameters are kept consistent, so the experimental measurement results basically reflect the feasibility of the analog hardware circuit.

In real circuit implementation, components such as resistors, capacitors exhibit non-ideal behaviors due to external factors like manufacturing tolerances and temperature variations. And also, parasitic capacitance and parasitic inductance will affect the frequency response and stability of the system, which are usually simplified or ignored in numerical simulations. In real circuits, some resistors need to be manually adjusted to show predicted dynamics. When aiming to large-scale neural networks, the distributed resistance

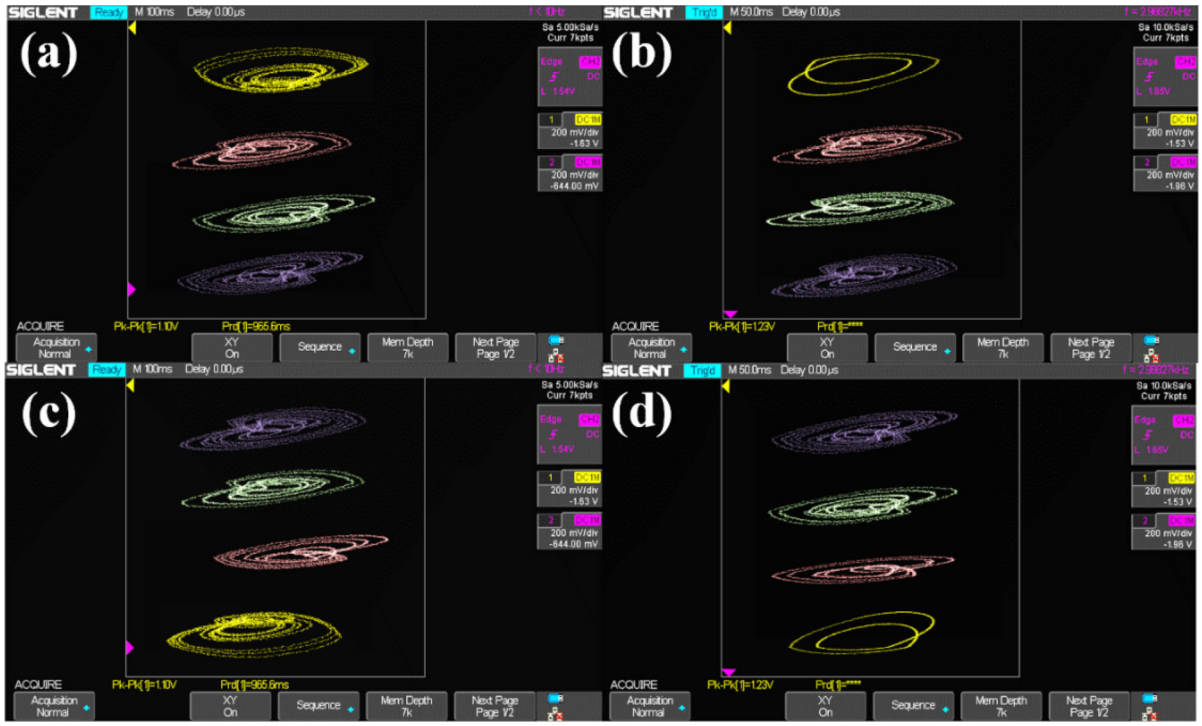

Fig. 18 Offset boosting observed on the oscilloscope by adjusting R_{11} under different initial conditions. $R_{11} = 5$ kΩ (yellow), $R_{11} = 3.2$ kΩ (pink), $R_{11} = 1.89$ kΩ (green), $R_{11} = 1.43$ kΩ (purple)

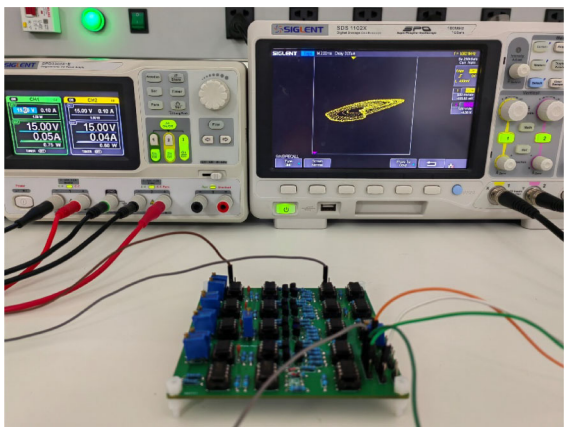

Fig. 19 The physical experimental setup

and the noise in circuit itself will significantly reduce the flexibility, stability and controllability. In future research we will focus on hybrid approaches, scalability studies, and long-term stability to meet these challenges.

6 Conclusion

A memristive HNN model with amplitude control and offset boosting is designed and analyzed, showing the complex brain-like dynamics. Various coexisting attractors can also be triggered under different initial conditions. The coupled weight of the memristor can rescale the amplitude of the firing of one neuron while keeping the other neuron unchanged. At the same time, one of the coefficients of the introduced memristor can also give amplitude control of the neuron firing leading to the offset boosting to the internal variable of the memristor. When broken symmetry occurs, multiple offset modes can be generated depending on the choice of initial conditions. Finally, a circuit experiment verifies the complex dynamics of the proposed model, including amplitude control and offset boosting. It shows that the non-bifurcation regulation can provide robust control on neuron dynamics without destroying other properties. Moreover, the concept of offset boosting has more possible applications in engineering, such as signal processing and metal electrolysis [51].

However, the model is primarily a theoretical one, the practical neuromorphic meaning remains to be demonstrated further. Additionally, we outlined potential applications of offset boosting in signal processing and metal electrolysis, but it needs to be rigorously tested in measurable real-world. Furthermore, the non-bifurcation regulation approach offers advantages in terms of stability and control. The stability and the flexibility need to be noticed and studied. Future studies are associated with the scalability of the model, particularly its performance in larger networks and its efficiency when deployed in physical neuromorphic hardware. In conclusion, this model presents a novel approach for controlling neural dynamics without bifurcation, which needs further observations in other practical real-world systems also.

Acknowledgements This work was supported financially by the National Natural Science Foundation of China (Grant No. 62371242), and a Project Funded by the Priority Academic Program Development of Jiangsu Higher Education Institutions.

Author contributions Xin Zhang: Writing—original draft, Methodology, Formal analysis. Chunbiao Li: Writing—review & editing, Conceptualization. Irene Moroz: Writing—review & editing, Supervision. Keyu Huang: Circuit, Formal analysis. Zuohua Liu: Validation.

Funding National Natural Science Foundation of China (Grant No.62371242), and a Project Funded by the Youth Talent Support Program of the China Association forScience and Technology (for Doctoral Students).

Data availability No datasets were generated or analysed during the current study.

Declarations

Conflict of interest The authors declare no competing interests.

References

1. Hopfield, J.J.: Neurons with graded response have collective computational properties like those of two-state neurons. Proc. Natl. Acad. Sci. **81**(10), 3088–3092 (1984)
2. Wilson, H.R.: Simplified dynamics of human and mammalian neocortical neurons. J. Theor. Biol. **200**(4), 375–388 (1999)
3. Hindmarsh, J.L., Rose, R.M.: A model of the nerve impulse using two first-order differential equations. Nature **296**(5853), 162–164 (1982)
4. Hodgkin, A.L., Huxley, A.F.: A quantitative description of membrane current and its application to conduction and excitation in nerve. J. Physiol. **117**(4), 500 (1952)
5. Lei, S., Xia, C., Li, Z., et al.: HNN: a novel model to study the intrusion detection based on multi-feature correlation and temporal-spatial analysis. IEEE Trans. Netw. Sci. Eng. **8**(4), 3257–3274 (2021)
6. Abernot, M., Todri-Sanial, A.: Training energy-based single-layer Hopfield and oscillatory networks with unsupervised and supervised algorithms for image classification. Neural Comput. Appl. **35**(25), 18505–18518 (2023)
7. Lee, S., Kim, J.: Two-step HNN-based pattern recognition combining DWT-based multi-resolution analysis for rechargeable cells distinction. IEEE Trans. Power Electron. **35**(11), 11891–11901 (2020)
8. Choi, W., Lee, C., Noh, S., et al.: Impact of operating temperature on pattern recognition accuracy of resistive array-based hardware neural networks. IEEE Electron Device Lett. **42**(5), 763–766 (2021)
9. Dong, Y., Zhang, H., Wang, C., et al.: Wind power forecasting based on stacking ensemble model, decomposition and intelligent optimization algorithm. Neurocomputing **462**, 169–184 (2021)
10. Varshney, S., Singh, T.P., Singh, A., et al.: A neuro-genetic Hopfield associative memory (HAM) with improved noise immunity. Mater. Today: Proc. **49**, 3482–3487 (2022)
11. Hu, B., Guan, Z.H., Xiong, N., et al.: Intelligent impulsive synchronization of nonlinear interconnected neural networks for image protection. IEEE Trans. Industr. Inf. **14**(8), 3775–3787 (2018)
12. Chen, C., Min, F., Zhang, Y., et al.: ReLU-type Hopfield neural network with analog hardware implementation. Chaos Solitons Fractals **167**, 113068 (2023)
13. Kong, X., Yu, F., Yao, W., et al.: Memristor-induced hyperchaos, multiscroll and extreme multistability in fractional-order HNN: Image encryption and FPGA implementation. Neural Netw. **171**, 85–103 (2024)
14. Lin, H., Wang, C., Xu, C., et al.: A memristive synapse control method to generate diversified multistructure chaotic attractors. IEEE Trans. Comput. Aided Des. Integr. Circuits Syst. **42**(3), 942–955 (2023)
15. Yu, F., Shen, H., Yu, Q., et al.: Privacy protection of medical data based on multi-scroll memristive Hopfield neural network. IEEE Trans. Netw. Sci. Eng. **10**(2), 845–858 (2023)
16. Yao, W., Liu, J., Sun, Y., et al.: Dynamics analysis and image encryption application of Hopfield neural network with a novel multistable and highly tunable memristor. Nonlinear Dyn. **112**, 693–708 (2024)
17. Sun, J., Li, C., Wang, Z., et al.: A memristive fully connect neural network and application of medical image encryption based on central diffusion algorithm. IEEE Trans. Industr. Inf. **20**(3), 3778–3788 (2024)
18. Sun, J., Zhai, Y., Liu, P., et al.: Memristor-based neural network circuit of associative memory with overshadowing and emotion congruent effect. IEEE Trans. Neural Netw. Learn. Syst. (2024). https://doi.org/10.1109/TNNLS.2023.3348553
19. Kanwisher, N., Khosla, M., Dobs, K.: Using artificial neural networks to ask 'why' questions of minds and brains. Trends Neurosci. **46**(3), 240–254 (2023)
20. Njitacke, Z.T., Isaac, S.D., Nestor, T., et al.: Window of multistability and its control in a simple 3D Hopfield neural network: application to biomedical image encryption. Neural Comput. Appl. **33**, 6733–6752 (2021)

21. Zhang, Y., Qiao, Y., Duan, L., et al.: Multistability of almost periodic solution for Clifford-valued Cohen-Grossberg neural networks with mixed time delays. Chaos Solitons Fractals **176**, 114100 (2023)
22. Ou, S., Guo, Z., Ci, J., et al.: Multistability of switched complex-valued neural networks with state-dependent switching rules. Neurocomputing **551**, 126499 (2023)
23. Yu, F., Kong, X., Yao, W., et al.: Dynamics analysis, synchronization and FPGA implementation of multiscroll Hopfield neural networks with non-polynomial memristor. Chaos Solitons Fractals **179**, 114440 (2024)
24. Lin, H., Wang, C., Yu, F., et al.: A triple-memristor Hopfield neural network with space multistructure attractors and space initial-offset behaviors. IEEE Trans. Comput. Aided Des. Integr. Circuits Syst. **42**(12), 4948–4958 (2023)
25. Yu, F., Kong, X., Mokbel, A.A.M., et al.: Complex dynamics, hardware implementation and image encryption application of multiscroll memeristive Hopfield neural network with a novel local active memeristor. IEEE Trans. Circuits Syst. II Express Briefs **70**(1), 326–330 (2023)
26. Tang, D., Wang, C., Lin, H., et al.: Dynamics analysis and hardware implementation of multi-scroll hyperchaotic hidden attractors based on locally active memristive Hopfield neural network. Nonlinear Dyn. **112**(2), 1511–1527 (2024)
27. Lai, Q., Yang, L., Chen, G.: Design and performance analysis of discrete memristive hyperchaotic systems with stuffed cube attractors and ultraboosting behaviors. IEEE Trans. Industr. Electron. **71**(7), 7819–7828 (2024)
28. Deng, Q., Wang, C., Lin, H.: Memristive Hopfield neural network dynamics with heterogeneous activation functions and its application. Chaos Solitons Fractals **178**, 114387 (2024)
29. Chen, C., Min, F., Zhang, Y., et al.: Memristive electromagnetic induction effects on Hopfield neural network. Nonlinear Dyn. **106**, 2559–2576 (2021)
30. Zhang, X., Li, C., Gao, X., et al.: Reproducing countless hidden attractors in a memristive system based on offset boosting. Eur. Phys. J. Plus **139**(2), 1–11 (2024)
31. Lin, H., Wang, C., Hong, Q., et al.: A multi-stable memristor and its application in a neural network. IEEE Trans. Circuits Syst. II Express Briefs **67**(12), 3472–3476 (2020)
32. Lai, Q., Wan, Z., Zhang, H., et al.: Design and analysis of multiscroll memristive hopfield neural network with adjustable memductance and application to image encryption. IEEE Trans. Neural Netw. Learn. Syst. **34**(10), 7824–7837 (2023)
33. Lin, H., Wang, C., Cui, L., et al.: Brain-like initial-boosted hyperchaos and application in biomedical image encryption. IEEE Trans. Industr. Inf. **18**(12), 8839–8850 (2022)
34. Ding, S., Wang, N., Bao, H., et al.: Memristor synapse-coupled piecewise-linear simplified Hopfield neural network: Dynamics analysis and circuit implementation. Chaos Solitons Fractals **166**, 112899 (2023)
35. Shrivastava, S., Keong, L.B., Pratik, S., et al.: Fully photon controlled synaptic memristor for neuro-inspired computing. Adv. Electron. Mater. **9**(3), 2201093 (2023)
36. Deng, Z., Wang, C., Lin, H., et al.: A memristive spiking neural network circuit with selective supervised attention algorithm. IEEE Trans. Comput. Aided Des. Integr. Circuits Syst. **42**(8), 2604–2617 (2023)
37. Ott, E., Grebogi, C., Yorke, J.A.: Controlling chaos. Phys. Rev. Lett. **64**(11), 1196 (1990)
38. Pyragas, K.: Continuous control of chaos by self-controlling feedback. Phys. Lett. A **170**(6), 421–428 (1992)
39. Wu, Q., Hong, Q., Liu, X., et al.: A novel amplitude control method for constructing nested hidden multi-butterfly and multiscroll chaotic attractors. Chaos Solitons Fractals **134**, 109727 (2020)
40. Zhang, X., Li, C., Huang, K., et al.: A chaotic oscillator with three independent offset boosters and its simplified circuit implementation. IEEE Trans. Circuits Syst. II Express Briefs **71**(1), 51–55 (2024)
41. Sayed, W.S., Roshdy, M., Said, L.A., et al.: Design and FPGA verification of custom-shaped chaotic attractors using rotation, offset boosting and amplitude control. IEEE Trans. Circuits Syst. II Express Briefs **68**(11), 3466–3470 (2021)
42. Ma, C., Mou, J., Xiong, L., et al.: Dynamical analysis of a new chaotic system: asymmetric multistability, offset boosting control and circuit realization. Nonlinear Dyn. **103**, 2867–2880 (2021)
43. Zhang, X., Li, C., Lei, T., et al.: Offset boosting in a memristive hyperchaotic system. Phys. Scr. **99**(1), 015247 (2023)
44. Li, C., Lei, T., Liu, Z.: Offset parameter cancellation produces countless coexisting attractors. Chaos **32**(12), 121104 (2022)
45. Bao, B., Hu, J., Cai, J., et al.: Memristor-induced mode transitions and extreme multistability in a map-based neuron model. Nonlinear Dyn. **111**(4), 3765–3779 (2023)
46. Li, C., Wang, R., Ma, X., et al.: Embedding any desired number of coexisting attractors in memristive system. Chin. Phys. B **30**(12), 120511 (2021)
47. Li, C., Chen, G., Kurths, J., et al.: Dynamic transport: from bifurcation to multistability. Commun. Nonlinear Sci. Numer. Simul. **95**, 105600 (2021)
48. Zhang, X., Li, C., Minati, L., et al.: Offset-dominated uncountably many hyperchaotic oscillations. IEEE Trans. Industr. Inf. **20**(5), 7936–7946 (2024)
49. Lai, Q., Guo, S.: Heterogeneous coexisting attractors, large-scale amplitude control and finite-time synchronization of central cyclic memristive neural networks. Neural Netw. **178**, 106412 (2024). https://doi.org/10.1016/j.neunet.2024.106412
50. Lai, Q., Wan, Z., Kuate, P.D.K.: Generating grid multi-scroll attractors in memristive neural networks. IEEE Trans. Circuits Syst. I Regul. Pap. **70**(3), 1324–1336 (2022)
51. Yang, J., Li, C., Zhang, Q., et al.: A memristive hyperchaotic oscillator with complete control and its application in the electrolysis of manganese. Chaos Solitons Fractals **183**, 114832 (2024)